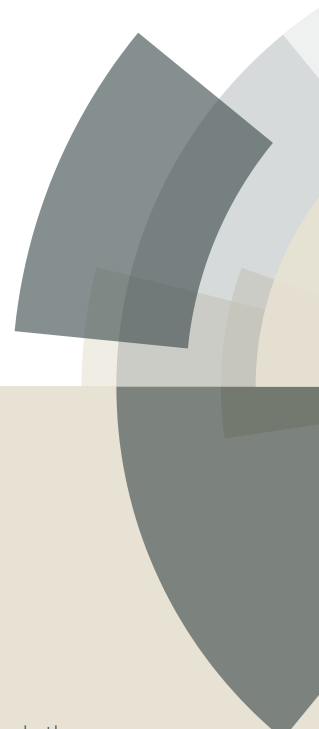


PCCP

Accepted Manuscript



This article can be cited before page numbers have been issued, to do this please use: S. Rajkumar, E. Elaiyappillai, G. K. S. B. Antony Paulraj, A. Sathiyar, M. B and P. M. Johnson, *Phys. Chem. Chem. Phys.*, 2019, DOI: 10.1039/C9CP02536G.



This is an Accepted Manuscript, which has been through the Royal Society of Chemistry peer review process and has been accepted for publication.

Accepted Manuscripts are published online shortly after acceptance, before technical editing, formatting and proof reading. Using this free service, authors can make their results available to the community, in citable form, before we publish the edited article. We will replace this Accepted Manuscript with the edited and formatted Advance Article as soon as it is available.

You can find more information about Accepted Manuscripts in the [author guidelines](#).

Please note that technical editing may introduce minor changes to the text and/or graphics, which may alter content. The journal's standard [Terms & Conditions](#) and the ethical guidelines, outlined in our [author and reviewer resource centre](#), still apply. In no event shall the Royal Society of Chemistry be held responsible for any errors or omissions in this Accepted Manuscript or any consequences arising from the use of any information it contains.

Electrochemical Performance of L-Tryptophanium picrate as an efficient electrode material for Supercapacitor Application

Rajkumar Srinivasan ^a, Elanthamilan Elaiyappillai ^a, S. Gowri ^{b,*}, A. Bella ^a, A. Sathiyar ^a, B. Meenatchi ^a, Johnson Princy Merlin ^{a,*}

^a Department of Chemistry, Bishop Heber College, Tiruchirappalli-620 017, Tamil Nadu, India.

^b Department of Physics, Cauvery College for Women, Tiruchirappalli-620 018, Tamil Nadu India.

Corresponding Authors:

1. J. P. Merlin

E-mail: pmej_68@yahoo.co.in

2. S. Gowri

E-mail: gow.1976@gmail.com

Abstract

A new, prominently stable organic material, L-Tryptophanium picrate was synthesized via a one-step process. The as-prepared sample was characterized by UV-visible, FT-IR, Raman, TGA-DSC, XRD, FE-SEM, EDX, ¹H-NMR, ¹³C-NMR and GC-MS. The significant capacitive behaviour of L-Tryptophanium picrate was investigated by Cyclic Voltammetric studies (CV), Galvanostatic Charge-Discharge test and Impedance Spectroscopy techniques in 1 M aqueous KOH. The newly fabricated L-Tryptophanium picrate electrode material exhibited excellent specific capacitance of 263 F g⁻¹ at current density of 1 A g⁻¹. Furthermore, it portrayed the capacitance retention of about 92% even after 2000 consecutive charge/discharge cycles. Moreover, the as-prepared electrode material illustrated electrochemically reversible behaviour. In addition, the synthesized material showed good electrochemical performance under the selected potential window. Thus, the fabricated electrode was proved to be a promising alternate electrode for high performance energy storage applications.

Keywords:

Cyclic Voltammetry, Supercapacitor, Charge-Discharge, Specific capacitance, L-Tryptophanium picrate

1. Introduction

View Article Online
DOI: 10.1039/C9CP02536G

The global climate change and the slow deterioration of natural resources have accelerated the development of technology associated with renewable energy conversion and storage^{1, 2}. Developing improved energy storage technology is highly significant with a view to extend the performance of portable electronics or to harvest renewable energy resources with many economic and environmental benefits. Among various energy storage devices, batteries and capacitors are typically regarded as the suitable choices to store energy by transforming chemical energy into electrical energy. Therefore, the development of energy-storage devices, primarily Supercapacitors (SC), have received great attention. These electrochemical capacitors play vital role in our day-to-day life, due to their unique chemical and physical properties such as power density, thermal stability, low-cost, longer cycle life and fast charge/discharge ability, compared to modern energy storage devices². They have been widely used in industrial power devices, digital communication devices, mobile phones, peak power sources, energy management etc.,³.

Generally, the energy storage mechanism of SC is classified into two types- Electric double layer capacitor (EDLCs), due to adsorption/separation of nanoscopic charges at the electrode-electrolyte interface and Pseudocapacitor (PCs), owing to fast-reversible Faradic charge transfer reactions⁴. Hybrid supercapacitors synergise these two-charge storage mechanisms, namely Faradic and non-Faradic reactions, resulting in improved device characteristics. The nature of the electrode material alters the storage mechanism. Recently researchers have explored the properties of several supercapacitor electrode materials and primarily focused on creating electrode materials with more ion-accessible surface sites, such as metal oxides, metal sulfides, metal hydroxides, porous carbon materials, conductive polymers, and their composites. But challenge lies in achieving high energy density materials⁵⁻⁷.

Indole compounds exist abundantly in living cells and function in various biologically important roles, primarily as tryptophan in proteins and indolealkylamines in serotonin and tryptamine etc. Because of the typical nature of indole ring, indole compounds tend to form the charge-transfer complexes with many aromatic acceptors such as pyridine, flavin and thiamine coenzymes and with nucleic acid bases⁸.

From 1969 onwards, organic materials were explored as electrodes for Electrochemical energy storage systems (EESSs), with the first report of an organic cathode material using dichloroisocyanuric acid. Thereafter, multiple research groups investigated a variety of organic small molecules such as quinones, dianhydrides, phthalocyanines and poly(acetylene) as cathode

materials, followed by many other conjugated polymers such as polypyrrole, polythiophene, polyaniline and their derivatives⁹. Furthermore, research on organic electrode materials has been revived due to the increased demand for low-cost high-performance energy storage system. However, the reported organic based electrode materials have their limitations such as low electrical conductivity, low specific capacitance low EDLC type capacitance and low mechanical/chemical stability, which reduce their applications in supercapacitors⁹.

To overcome these issues of organic based electrode materials, the design of new type of organic materials gained momentum, in which the redox pathway can additionally provide pseudocapacitance with sufficiently large space as the diffusion channels of electrode ions. Zhuoxin Liu group reported the design of a novel Soft Device-Level, Dynamically Super-Tough Supercapacitor with an Energy-Dissipative Dual-Crosslinked Hydrogel Electrolyte¹⁰. This super tough supercapacitor was found to have great potential in wearable applications. *R.S. Hastak* et al. successfully synthesised activated carbon (AC) and phosphoric acid doped poly[2,5 benzimidazole] (ABPBI), with better electrochemical performance¹¹. *Bidhan* et al. fabricated a new type of benzimidazole based COF, with a high specific capacitance of 335 F g⁻¹ with 93% retention after 1000 cycles¹². *Yan Huang* et al. fabricated a polypyrrole based supercapacitor with excellent cyclic stability and superior pseudocapacitance with specific capacitance of 214 F g⁻¹¹³.

H. Jeong group successfully synthesized amino acid derived N-doped carbon material as electrode material with the specific capacitance of 58 F g⁻¹ at current density of 0.1 A g⁻¹ with 2000 cycling stability¹⁴. Very recently directly electrodeposited of imidazole modified poly(pyrrole) copolymers were utilised as electrode material, which exhibited the specific capacitance 201 F g⁻¹ at 10 mVs⁻¹¹⁵. Although the organic based electrode materials have good electrochemical performance due to redox active species, the number of related reports highlighting the structural characteristics is still limited. Therefore, in order to develop an organic based electrode material with notable supercapacitive performance, an alternate organic material with a favourable structure is designed in the present work, to ensure pseudocapacitive process with facile electrolyte diffusion and fast electron transfer^{9, 16}.

Recently several kinds of L-tryptophan derivatives and L-tryptophan based metal oxides were used as functional materials in sensor applications^{17, 18}. The charge-transfer interactions were shown to play an important part. In addition, L-tryptophan exhibits photochromism and thermochromism, which elevate its scope and potential usage in optoelectronics and sensors¹⁸. The

literature scanning showed that few tryptophan-based materials had been tested as electrode materials in energy storage applications.

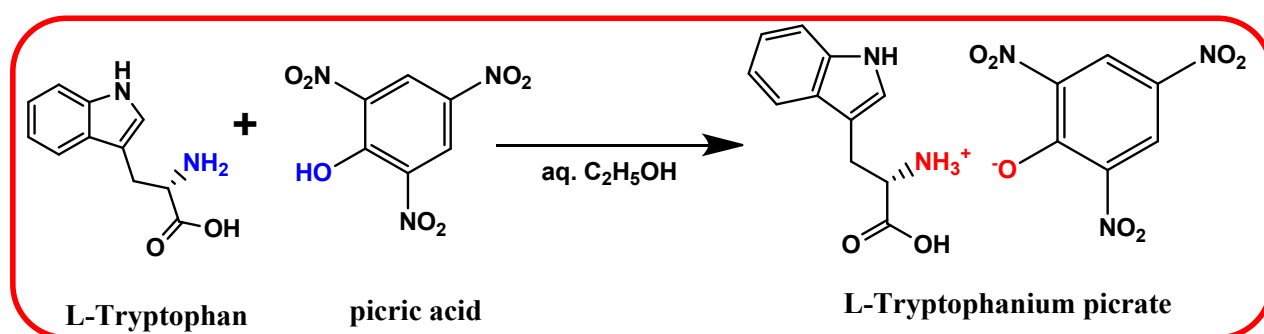
Thus, in the present work, a new, remarkably stable tryptophan derivative namely, L-Tryptophanium picrate was prepared by a simple, one-step route via two components acid-base reaction between L-tryptophan and picric acid in high yield under ambient condition. The title compound has not been examined as an electrode material in SC application so far. Herein, we report, a systematic study of evaluation of L-Tryptophanium picrate as an effective, sustainable, cheap and scalable electrode material for energy storage applications.

2. Experimental Methods

2.1. Materials

L-Tryptophan, Picric acid, Carbon black, Polyvinylidene difluoride (PVdF), N-methyl-2-pyrrolidone (NMP), nickel foil, KOH and Ethanol were purchased from Merck and used as procured. All the reagents used were of analytical grade.

2.2. Preparation of L-Tryptophanium picrate



Scheme 1: Synthesis of L-Tryptophanium picrate

The reddish needle shaped crystalline compound of L-Tryptophanium picrate was purified with water-acetone mixture and then vacuum dried (Scheme 1).

2.3. Characterization techniques

IR and Raman spectra were performed by Bruker Vector 22 spectrophotometer and Bruker RFS 27: Standalone FT-Raman spectrophotometer respectively. XRD analyses were done using Shimadzu XRD 6000 (Japan), respectively. The UV-vis spectrum was recorded using Perkin-Elmer Lambda 35 UV/Vis spectrometer. The FE-SEM and Energy Dispersive X-ray (EDX) were captured by means of Hitachi SU6600. ^1H - and ^{13}C - NMR spectral analyses were done by Bruker AVANCE

III 500 MHz (AV 500) multi nuclei solution NMR Spectrometer. TGA and DSC analyses were carried out using TG analyzer NETZSCH STA 449 F3 Jupiter and DSC 6000 respectively. GC-MS analysis was performed by SHIMADZU/ QP2020. Supercapacitor studies were performed using Princeton Applied Research (VSP-1) Electrochemical work station.

2.4. Fabrication of Electrode Material

With a view to analyse the electrochemical performance of the fabricated electrode of L-Tryptophanium picrate, CV, Galvanostatic Charge-Discharge and impedance techniques were employed in aqueous 1 M potassium hydroxide (electrolyte), with the three-electrode assembly of platinum wire (counter electrode), Ag/AgCl (reference electrode) and L-Tryptophanium picrate coated Nickel foil (working electrode). The Cyclic voltamogram was recorded in the potential range of 0 to 0.64 V at different scan rates (5 to 100 mVs⁻¹). Subsequently, galvanostatic charge/discharge studies were also achieved at different current densities (1 to 5 A g⁻¹). Further, EIS was recorded in the frequency range from 100 kHz to 0.1 Hz with an amplitude of 10 mV AC voltage using Ag/ AgCl/ KCl (sat'd) (reference electrode) in the potential range of -1 V to +1 V.

In order to design the working electrode, the nickel foil was pre-treated sequentially with acetone, 1 M HCl, absolute ethanol and deionized water for 20 mins to ensure the clean surface. Then the slurry, prepared by mixing 80% L-Tryptophanium picrate (active material), 10% carbon black and 10% poly(vinylidene)difluoride (PVDF), with N-methyl-2-pyrrolidone as solvent was coated on nickel foil (1 cm × 1 cm). The L-Tryptophanium picrate coated electrode was dried in a hot air oven for 6 hours and then the electrode weight was measured to determine the amount of L-Tryptophanium picrate coated on the nickel foil. The characteristic mass of the fabricated electrode material was found to be 0.002 g. The specific capacitance (C_{sp}) values were evaluated from CV and GCD measurements using equations (1) and (2), respectively

$$C_{sp} = \frac{\int idv}{2 \times S \times \Delta V \times m} \dots \dots \dots (1)$$

$$C_{sp} = \frac{I \times \Delta t}{m \times \Delta V} \dots \dots \dots (2)$$

Where, $\int idV$ indicates the integral area of one complete cycle of CV curve, ΔV potential window (V), 'm', mass of the active material (mg), S, scan rate (mV/s), I (A), discharge current and Δt (s), the discharge time.

3. Results and Discussion

View Article Online
DOI: 10.1039/C9CP02536G

3.1. FT-IR Analysis

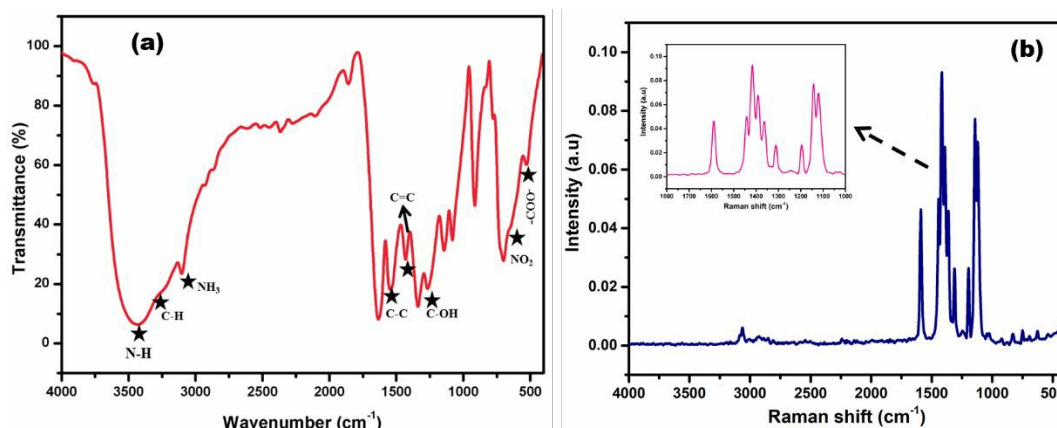


Fig. 1: a) FT-IR and b) Raman spectrum of L-Tryptophanium picrate

Fig.1a depicted a series of bands from 4000 to 400 cm^{-1} . The absorption frequency at 3430 cm^{-1} was labelled to N–H stretching of indole group. Moreover, the wider band at about 3300–2700 cm^{-1} was probably due to $\nu_{\text{N-H}}$ of NH_3^+ groups, $\nu_{\text{C-H}}$ of aromatic ring and $\nu_{\text{C-H}}$ of CH_2 aliphatic groups. Thus, the carbon–hydrogen stretching vibrations displayed bands around 3000–3100 cm^{-1} . The broadband at 1634 cm^{-1} was assigned to the asymmetric NH_3^+ deformation mode. The stretching frequency observed at 1554 cm^{-1} was the signature of C–C bond. As expected, C–H in-plane bending vibration was observed between 1000–1300 cm^{-1} . The strong intense band at 1271 cm^{-1} was owing to in-plane C–H bending vibration. The C–H out of plane vibrations were noted in the region 675–1000 cm^{-1} . The stretching frequency at 638 cm^{-1} was assigned to C–C–C deformation band of the phenyl ring¹⁹.

The characteristic frequencies of 1634 and 1595 cm^{-1} were assigned as the signature peaks of asymmetric stretching of carboxylate group and asymmetric deformation of the NH_3^+ group. Significantly, it is noticed that they are mainly due to ring vibrations of the picrate anion and 2,4,6-trinitrophenol^{20, 21}. Hence the IR spectrum of L-Tryptophanium picrate provided substantial structural conformation.

3.2. Raman spectral analysis

The characteristic moderate band in Raman spectrum of L-Tryptophanium picrate (Fig. 1b) at 3158 cm^{-1} was ascribed to the N-H stretching of indole group. It is noticed that these lines are superimposed on the broad bands between 3300–2500 cm^{-1} , which were attributed to stretching of N-H bonds of NH_3^+ group²¹. The prominent band at 3102 cm^{-1} was the signature band of stretching

mode of C-H bond of pyrrole ring. The weak band at 2934 cm^{-1} was owing to O-H stretching vibration. The bands observed at 1442 cm^{-1} and 1428 cm^{-1} were suggestive of the deformation scissoring vibration of CH_2 group. The band at 1416 cm^{-1} was labelled as the symmetric stretching of COO^- (carboxylate) group. Additionally, the very strong band at 3060 cm^{-1} due to C-H stretching and the bands at 1600 , 1024 , 1044 cm^{-1} due to $\nu_{\text{C}-\text{C}}$ of benzene ring were supportive of L-Tryptophanium picrate structure^{21,22}.

3.3. UV-Vis Spectral Study

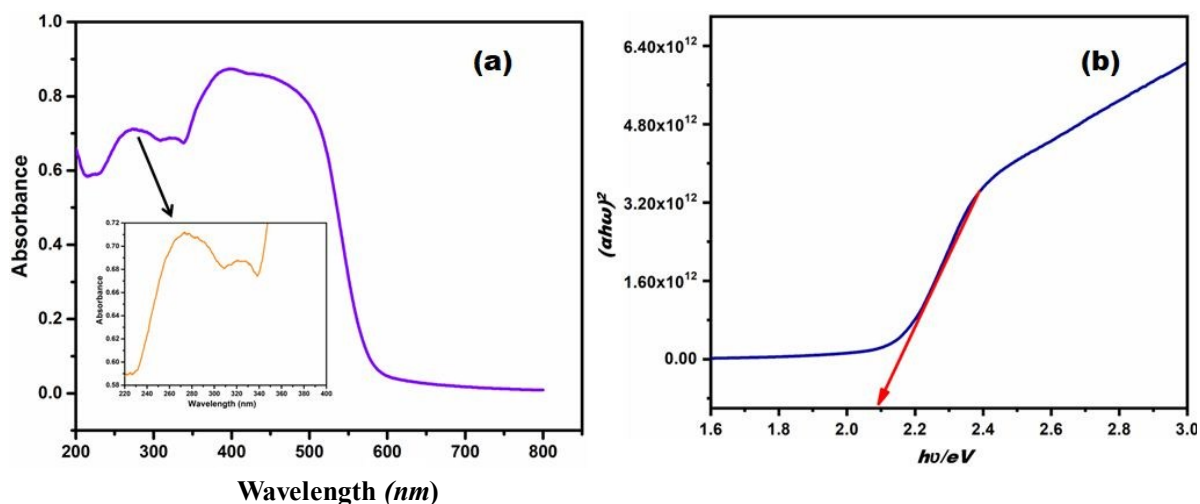


Fig. 2: a) UV-vis and b) Tauc plot of L-Tryptophanium picrate

The UV-vis spectrum of the L-Tryptophanium picrate (Fig.2a) showed the absorption maximum at 280 nm owing to its charge transfer intermolecular $\pi \rightarrow \pi^*$ transitions and a shoulder observed at 327 nm was assigned to the transitions taking place in tryptophan and picric acid moiety^{23,24}. The experimental energy gap (E_g) of L-Tryptophanium picrate has been calculated using Tauc plot (Fig.2b) and E_g was calculated as 2.08 eV. All these evidences are supportive of the suggested structure and the characteristic features of L-Tryptophanium picrate.

3.4. Electrochemical Properties

View Article Online
DOI: 10.1039/C9CP02536G

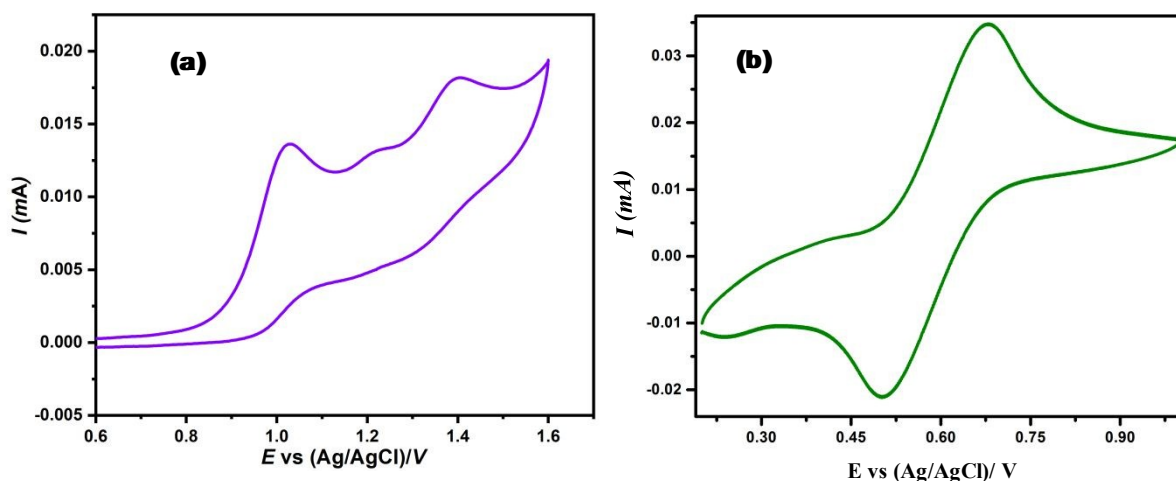


Fig. 3: a) CV of L-Tryptophanium picrate in DMSO (0.5 mM) at 50 mVs⁻¹
b) CV of standard Ferrocene (0.1 mM) at 50 mVs⁻¹

The corresponding HOMO levels were calculated using $E_{\text{ox}}(\text{onset})$ obtained from cyclic voltammogram of L-Tryptophanium picrate in DMSO (Fig.3a) using the empirical relation $E_{\text{HOMO}} = [(E_{\text{ox}} - E_{1/2(\text{ferrocene})}) + 4.8]$ eV. Ferrocene was used as external standard while recording CV. The CV of L-Tryptophanium picrate exhibited two anodic peaks at 0.65 V and 0.5 V (Fig.3b). $E_{1/2}$ of ferrocene (0.59 V) was used to calculate E_{HOMO} and E_{HOMO} was found to be -5.41 eV. Further, using the calculated HOMO value and the λ_{onset} value from UV absorption spectrum, the LUMO energy was evaluated by the empirical relation $E_{\text{LUMO}} = (1240/\lambda_{\text{onset}}) - E_{\text{HOMO}}$. Thus, E_{LUMO} was calculated as -3.20 eV and the calculated energy gap (E_g) of the L-Tryptophanium picrate was 2.21 eV²⁵.

3.5. DFT-TDDFT study

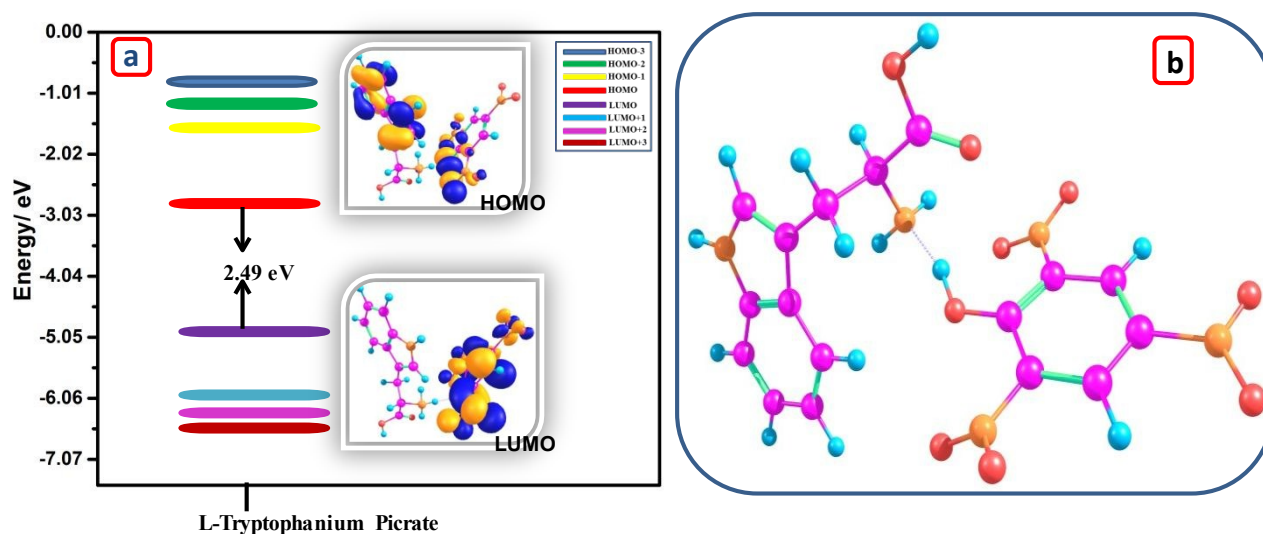


Fig.4: a) DFT-Frontier Molecular Orbitals (FMO) and Energy Level Diagram of L-Tryptophanium picrate b) Optimized Geometry of L-Tryptophanium picrate

View Article Online

DOI: 10.1039/C9CP02536G

To understand the relationship between geometric configuration and electrochemical performance of L-Tryptophanium picrate, Density Functional theory (DFT) simulations were performed. The ground state (S_0) geometry of L-Tryptophanium picrate was optimized with Gaussian 09 package²⁶ at B3LYP/6-31+G (d,p) level²⁷⁻³³. The Calculated vibrational frequency analysis confirms that the optimized geometry corresponds to minima on the potential energy surface. The ground state geometry and frontier orbital distribution of L-Tryptophanium picrate are presented in Fig.4a-b.

The HOMO-LUMO energy gap calculated by DFT analysis for L-Tryptophanium picrate was found to be 2.49 eV, which is observed to be much closer with the experimentally derived band gap value of 2.21 eV through CV. Moreover, the analysis predicts the HOMO energy level of L-Tryptophanium picrate as -6.01 eV and LUMO as -3.52 eV. It is worth mentioning that the electron charge distribution of HOMO orbitals is more on the indole and picrate group whereas LUMO's are mainly spread over the picrate group. Hence, it sufficiently explains the fact that conduction electrons are originated mainly from Tryptophan moiety with lesser contribution from picrate moiety. The UV-visible spectrum of L-Tryptophanium picrate calculated by Time Dependent-DFT (TD-DFT) method with the suitable cam-B3LYP/6-31+G (d,p)³⁴ level of basis set was observed to be 324 nm which is close to the experimentally obtained UV-vis spectrum of L-Tryptophanium picrate (327 nm) Fig. S1.

IR stretching calculated for L-Tryptophanium picrate is similar to experimentally obtained IR spectrum of L-Tryptophanium picrate in Fig.S2. Furthermore, IR stretching frequency of L-Tryptophanium picrate with $N_{40}-H_{41} \cdots O_{31}-H_{42}$ stretching band obtained at 1637 cm^{-1} , closely matches to the experimentally obtained value of 1634 cm^{-1} , thereby supports that the NH_3^+ in tryptophan is in close proximity with the picrate moiety.

3.6. Thermal and XRD Analysis

View Article Online
DOI: 10.1039/C9CP02536G

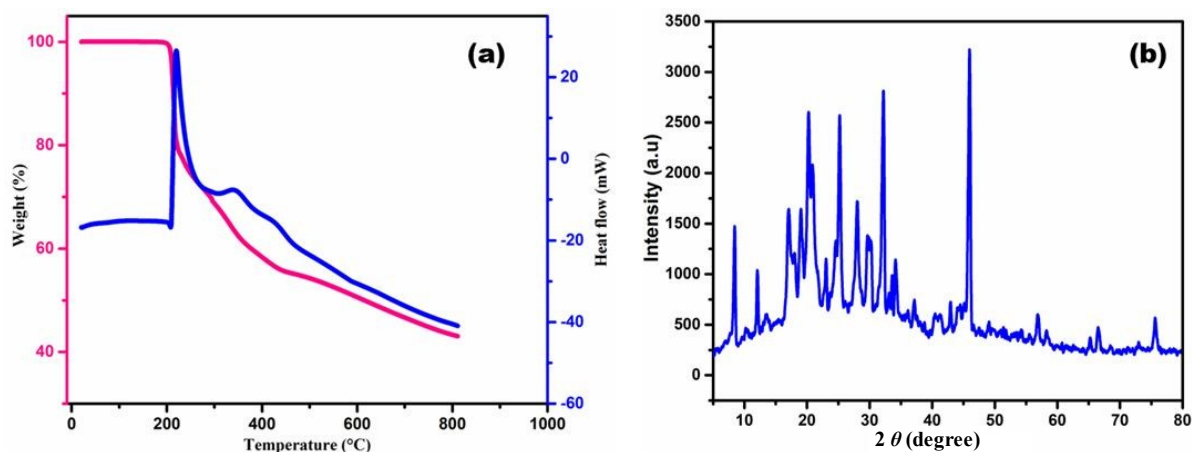


Fig.5: a) TGA- DSC Curve of L-Tryptophanium picrate b) XRD pattern of L-Tryptophanium picrate

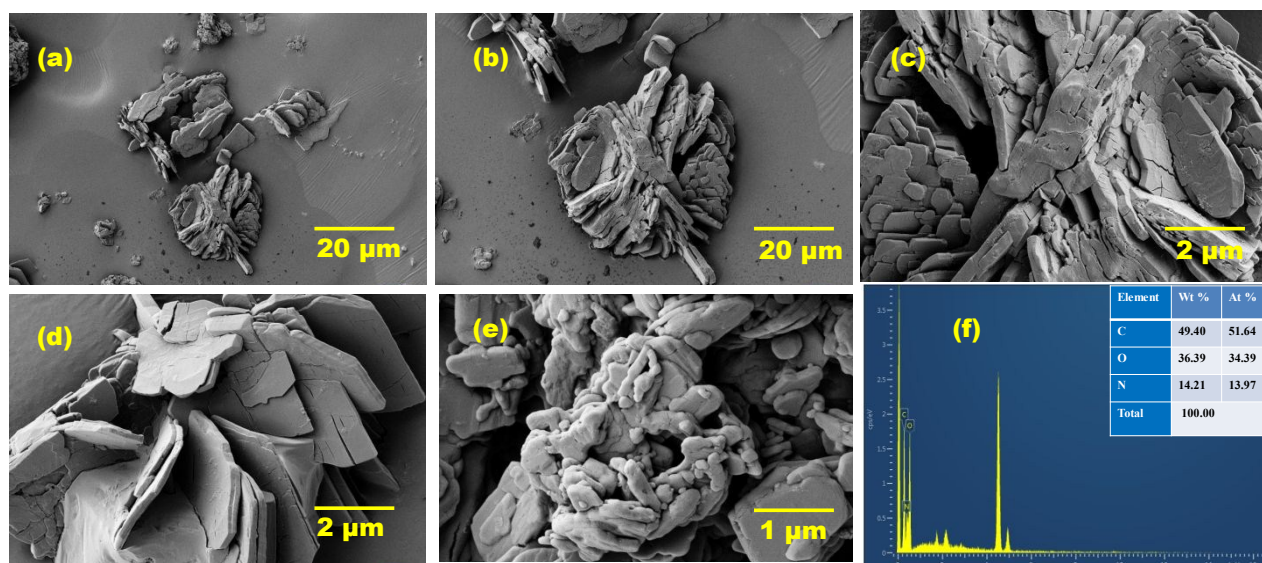
Fig.5a shows the TGA-DSC curve of L-Tryptophanium picrate. The pattern noticed in TGA-DSC curve provided the vital information about the thermal stability of L-Tryptophanium picrate. The observations were made in nitrogen atmosphere (at a heating rate of 20°C from 30–800°C) (Fig.5a). The initial mass of L-Tryptophanium picrate was 2.79 mg and the last mass left out after the experiment was 2.01 % from the initial mass at 800°C, suggesting the major decomposition of the sample. Moreover, the curve portrayed a two-step decomposition, suggesting that the melting was followed by decomposition, between 200°C to 800°C. The first stage decomposition with the weight loss of 56.88 % occurred at 197°C. Further, it indicates that there is no phase transition before melting¹⁹.

Fig.5a indicates the melting point (T_m) as 220°C. There is a gradual and significant weight-loss as the temperature was increased above the melting point. It is seen that at different stages, various gaseous fractions like CO, CO₂, NH₃ etc., were liberated and the total decomposition of the compound took place at about 800°C. The subsequent decomposition pathway of L-Tryptophanium picrate clearly indicates its high structural stability and therefore suggests that it can withstand high temperature during device operation³⁵.

The XRD pattern of L-Tryptophanium picrate is presented in Fig.5b. The peaks are located at $2\theta = 7.95^\circ, 15.94^\circ, 32.24^\circ, 37.11^\circ$ and 45.97° , which matched with the peaks observed in the case of L-tryptophan (JCPDS cards file no. 25-1960) and picric acid (JCPDS cards file no. 03-0484). These values agreed well with the reported values and hence this observation supports the clear signature of indole moiety in L-Tryptophanium picrate as reported by Gowri et al^{18, 19}.

3.7. FE-SEM and EDX Analysis

View Article Online
DOI: 10.1039/C9CP02536G



**Fig. 6: a-e) FE-SEM Images of L-Tryptophanium picrate at different magnifications
f) EDX analysis of L-Tryptophanium picrate**

The surface morphological images of the freshly prepared L-Tryptophanium picrate (Fig. 6a-e), showed disassembly of nanolayers like morphology. The observed L-Tryptophanium picrate nanolayers could provide the prominent electro-active sites for charge-transfer processes, at the electrode-electrolyte interfaces. In Fig. 6f, the recorded EDX spectrum exhibited elemental peaks only for C, N, O and thus substantiating the presence of the important elements in the as-synthesized L-Tryptophanium picrate sample.

3.8. NMR & GC-MS Analysis

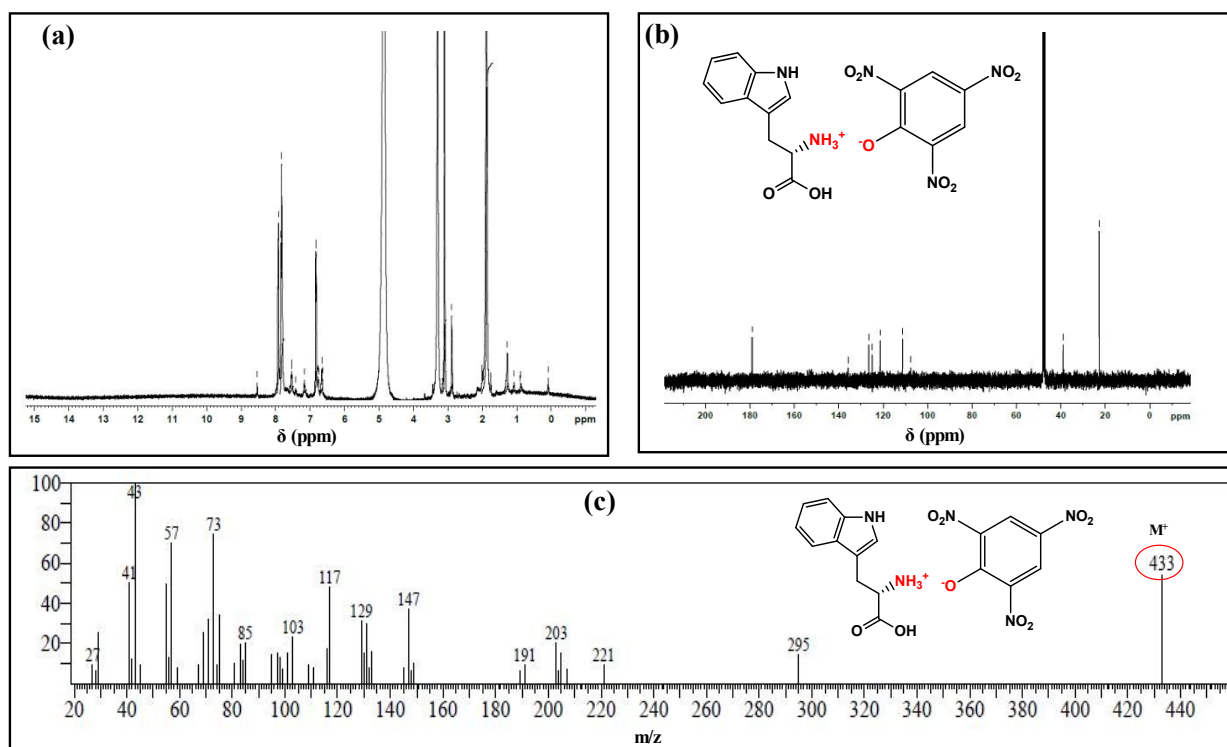
View Article Online
DOI: 10.1039/C9CP02536G

Fig.7: a) ¹H-NMR and b) ¹³C-NMR c) GC-MS spectrum of L-Tryptophanium picrate

The ¹H and ¹³C- NMR spectrum of L-Tryptophanium picrate are shown in Fig.7 (a) and (b) respectively. The chemical shift values (δ) of the protons of L-Tryptophanium picrate are plotted on the X-axis and the intensity is plotted on the Y-axis (Fig.7a). The multiplets appeared between δ 7-7.2 ppm were attributed to the aromatic protons of tryptophan moiety. The doublets observed at δ 7.55 and 7.42 ppm were owing to the similar kind of protons in picric acid moiety, whereas in bare picric acid, the same appeared at δ 8.53 ppm. This upfield shift of frequency accounts for the increase of electron density, owing to charge transfer in the synthesized material. The appearance of new chemical shift value at δ 8.75 ppm was ascribed to [NH₂-H]⁺ proton. Moreover, it confirms the transfer of -OH proton to the nitrogen atom of tryptophan ³⁶.

In ¹³C-NMR spectrum of L-Tryptophanium picrate (Fig.7b), the signal at δ 179.05 ppm was assigned to aromatic carbon present in the picrate ion. The series of peaks at δ 124.89, 126.53, 113.3 and 135.87 ppm were ascribed to carbon in aromatic rings. The solvent peak appeared at 40 ppm. Thus, NMR (¹H and ¹³C) spectral analysis provided the useful information about the various carbon and hydrogen environments prevailing in the molecular structure of L-Tryptophanium picrate ^{37, 38}. The GC-MS spectrum (Fig.7c) also confirms the formation of L-Tryptophanium picrate, by exhibiting the intense peak at m/z = 433.00 (calculated m/z for L-Tryptophanium picrate= 433.09).

3.9. Electrochemical capacitance measurements

3.9.1. Capacitance measurement using CV

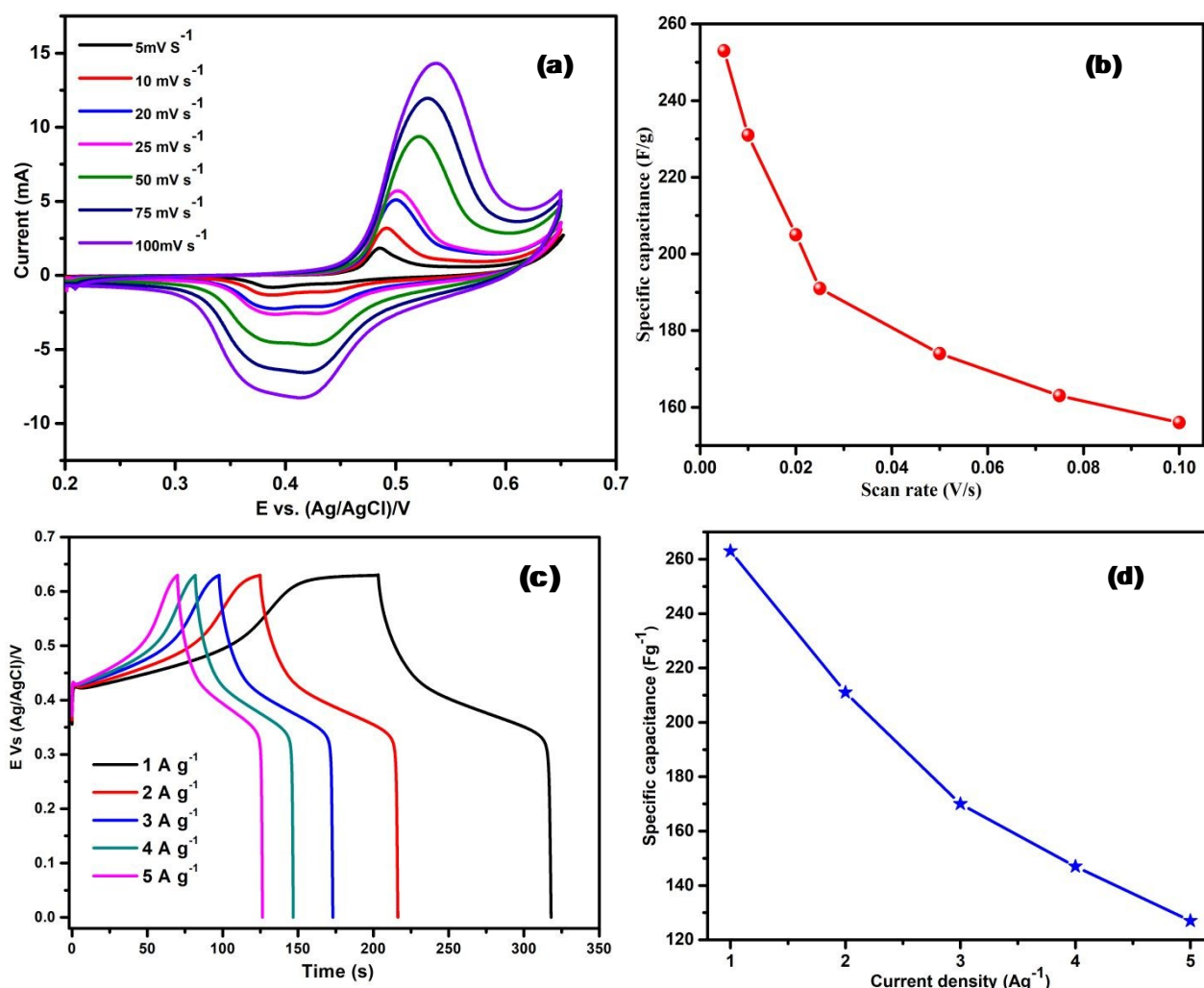
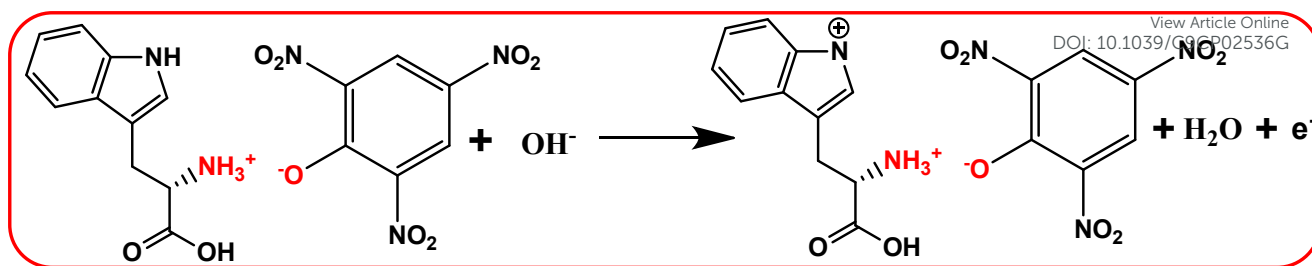


Fig. 8: a) CV curves of L-Tryptophanium picrate at various scan rates in 1M aqueous KOH
b) Specific capacitance of L-Tryptophanium picrate as a function of Scan rate
c) GCD curves of L-Tryptophanium picrate at different current density
d) Specific Capacitance of L-Tryptophanium picrate as a function of Current density

Fig.8a shows the CV curve of the L-Tryptophanium picrate electrode recorded at different scan rates in the potential range of 0 to 0.64 V. The calculated specific capacitance values were 253, 231, 205, 191, 174, 163 and 156 F g⁻¹ at 5, 10, 20, 25, 50, 75 and 100 mVs⁻¹ scan rate respectively, (Fig.8a). A pronounced redox peak, characteristic of the pseudocapacitive behaviour was noted for L-Tryptophanium picrate electrode material, due to the redox reaction³⁹. The probable redox pathway of L-Tryptophanium picrate electrode accounting for its supercapacitive behaviour is displayed in Scheme 2. Moreover, redox peaks are nearly symmetrical in nature, revealing the predominant reversibility of the redox electrode.



Scheme 2: Redox pathway of synthesized material as modified electrode

Fig.8b, displays the effect of scan rate on the specific capacitance (C_{sp}) value. A noticeable decrease in specific capacitance with scan rate, was observed. Only a very slight change in shape of the plot was identified and hence it is further suggestive of good kinetic reversibility of the synthesized electrode material. From this plot, it is observed that increase of scan rate decreased the specific capacitance value, mainly due to ion-exchange storage mechanism³⁹⁻⁴¹. This type of behaviour reflects the fact that an electrochemical process might easily occur at low scan rates and furthermore it confirms that the charge storage mechanism is a diffusion controlled redox reaction. With the increase of scanrate, the anodic peak potential (E_{pa}) and cathodic peak potential (E_{pc}) were found to be slightly shifted towards positive and negative potentials respectively, attributed to the polarization effect in addition to ion diffusion. The excellent capacitive behaviour of L-Tryptophanium picrate originates from the pseudocapacitive behavior, owing to the more redox sites in the synthesized material.

3.9.2. Capacitance Measurement using GCD

The typical GCD curves of L-Tryptophanium picrate electrode recorded at five different current densities in the potential range of 0 to 0.64 V are shown in Fig.8c, which further indicate the pseudocapacitive electrochemical performance. Apparently, the electro-active L-Tryptophanium picrate electrode delivered C_{sp} of 263, 211, 170,147 and 127 F g⁻¹ at current density of 1, 2, 3, 4 and 5 A g⁻¹ respectively (Fig. 8c). The obtained charge-discharge curves of L-Tryptophanium picrate electrode showed dependence on applied current density⁴². The recorded charge/ discharge plot exhibited a distinct plateau in the charging and discharging processes and a few voltage drops indicated the Faradic behaviour of the reaction and also the superior rate capability. Fig.8d reveals that the C_{sp} value is indirectly related with current density, thereby following the same trend as noted in the case of CV analysis^{43,44}. In view of the above observations, it is noticed that the electrochemical performance of L-Tryptophanium picrate in terms of specific capacitance is significantly better than that of other organic based materials described in the literature (Table 1).

Table 1: Comparison of the Electrochemical Performance of Organic based Electrode Materials

New Article Online
DOI: 10.1039/C9CP02536G

Electrode Materials	Electrolyte	Specific Capacitance	Cycle Number	Capacitance retention	Current density	Ref. No
His-NCMs	6 M KOH	58 F g ⁻¹	2000	-	0.1 A g ⁻¹	14
ANEG	1 M KOH	115 F g ⁻¹	1000	93 %	4 A g ⁻¹	45
N-MCNF	Ionic liquid	204 F g ⁻¹	32500	-	0.25 A g ⁻¹	46
CNT@Mn-MOF	1 M Na ₂ SO ₄	203.1 F g ⁻¹	3000	88 %	1 A g ⁻¹	47
β-ketoenamine-linked COF	1 M H ₂ SO ₄	48 F g ⁻¹	5000	85 %	0.1 A g ⁻¹	48
β-ketoenamine-linked Conjugated micro Porous Polymer	1 M H ₂ SO ₄	252 F g ⁻¹	10000	-	1 A g ⁻¹	49
Ni-pPDA/GC	1 M KOH	184.7 F g ⁻¹	5000	80 %	1 A g ⁻¹	50
Mn-pPDA/GC	1 M KOH	109.9 F g ⁻¹	5000	97 %	1 A g ⁻¹	50
TpPa-COF@PANI	1 M H ₂ SO ₄	95 F g ⁻¹	30000	83 %	0.2 A g ⁻¹	51
NiBDZ	1 M H ₃ PO ₄	127.87 F g ⁻¹	-	-	-	52
BiBDZ	1 M H ₃ PO ₄	88.6 F g ⁻¹	5000	93.61 %	0.5 A g ⁻¹	52
BNC capsules	0.1 M KOH	230 F g ⁻¹	1000	-	5 A g ⁻¹	53
PPY-based	1 M H ₃ PO ₄	214 F g ⁻¹	10000	98 %	0.5 A g ⁻¹	13
TPT-DAHQ	1 M KOH	256 F g ⁻¹	2000	98 %	0.5 A g ⁻¹	54
L-Tryptophanium Picrate	1 M KOH	263 F g⁻¹	2000	92 %	1 A g⁻¹	This work

3.9.3. Electrochemical Impedance Spectroscopic Analysis

View Article Online
DOI: 10.1039/C9CP02536G

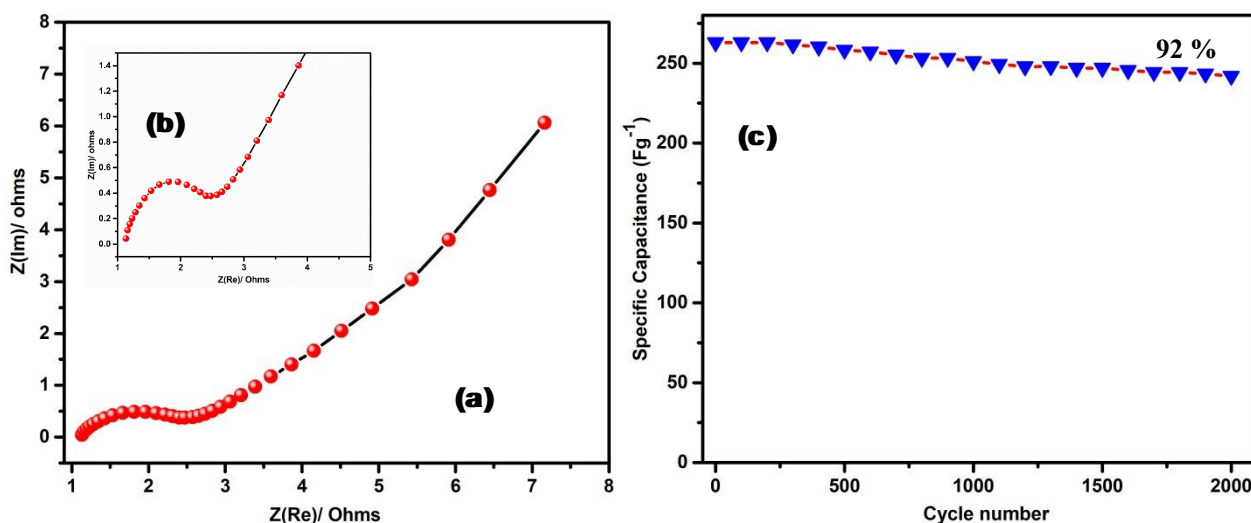


Fig. 9: a) Nyquist Plot of L-Tryptophanium picrate at 10mV AC voltage
b) Magnified Nyquist plot of L-Tryptophanium picrate
c) Cyclic stability of L-Tryptophanium picrate

The EIS plot of the fabricated electrode material represented the typical Nyquist plots at the open circuit potential (Fig.9a). Generally, the diameter of the semi-circular region denotes the charge transfer resistance. The curve consists of the electrolyte resistance (R_s) and charge transfer resistance (R_{ct}). In Fig.9b shows the magnified view of Nyquist plot of L-Tryptophanium picrate, which possesses a small semicircle produced by the polarization effect. At lower frequency, a straight line was detected, which might be due to the mass transfer effect. From Fig.9a, it is found that L-Tryptophanium picrate exhibited small Equivalent Series Resistance (ESR) value of 2.49Ω , which promotes electrolyte diffusion into the active electrode surface. The appearance of straight line at low frequency portion of the plot suggests that an extraordinary capacitive behavior of synthesized electrode material. Thus, the EIS analysis is also evident of the supercapacitive nature of as-synthesized L-Tryptophanium picrate^{27, 55, 56}.

3.10. Stability Measurement

The stability measurement of L-Tryptophanium picrate electrode was examined by 2000 consecutive GCD cycles at 1 A g^{-1} current density. The C_{sp} value of L-Tryptophanium picrate shows 92% retention even after 2000 GCD cycles (Fig.9c). The effective ion diffusion between L-Tryptophanium picrate and KOH interfaces is predominantly accountable for the enhanced cycling stability. Hence, the electrochemical studies (CV, GCD and EIS) proved that L-Tryptophanium picrate has promising behaviour as electrode material for supercapacitor applications. This

capacitive behaviour of L-Tryptophanium picrate is mainly attributed to its effective and abundant redox sites with high thermal stability.

However, the as-fabricated L-Tryptophanium picrate electrode material exhibited the comparable C_{sp} value with the reported works. Thus, the electrochemical performance of the L-Tryptophanium picrate electrode can be enhanced by increasing the surface area, porosity, morphology, when the dopants adding such as conducting polymers based, metal/ metal oxides based and carbon based materials^{50, 54, 57-66}.

4. Conclusion

In summary, the new, cheap and easily scalable electrode material, L-Tryptophanium picrate synthesized and investigated for its applicability as an electrode material in supercapacitors. The L-Tryptophanium picrate showed high capacitance of 263 F g^{-1} at the current density of 1 A g^{-1} in 1M aqueous KOH and it retained 92 % of its initial specific capacitance even after 2000 GCD cycles at 1 A g^{-1} . Moreover, the fabricated electrode material exhibited high specific capacitance with outstanding long-term cyclic performance at ambient conditions. Additionally, DFT calculations were performed to view the optimized HOMO-LUMO energy level of L-Tryptophanium picrate and to calculate the theoretical energy gap. Thus, the comparison of experimental and computational data proves that the notable L-Tryptophanium picrate has the optimal band gap, suitable for sustainable energy storage devices. These findings have proved that the as-synthesized L-Tryptophanium picrate is a better electrode material for supercapacitor applications.

Acknowledgement

The authors thank the Management of Bishop Heber College (Autonomous), Tiruchirappalli-620 017, Tamil Nadu, India for the support and facilities provided through DST-FIST Instrumentation Centre at Bishop Heber College (HAIF). Mrs. A. Bella sincerely acknowledges DST for the financial support under DST-WOSA Scheme- File. No. SR/ WOS-A / CS-22/ 2016.

Conflicts of Interest

The authors have no conflicts to declare.

References

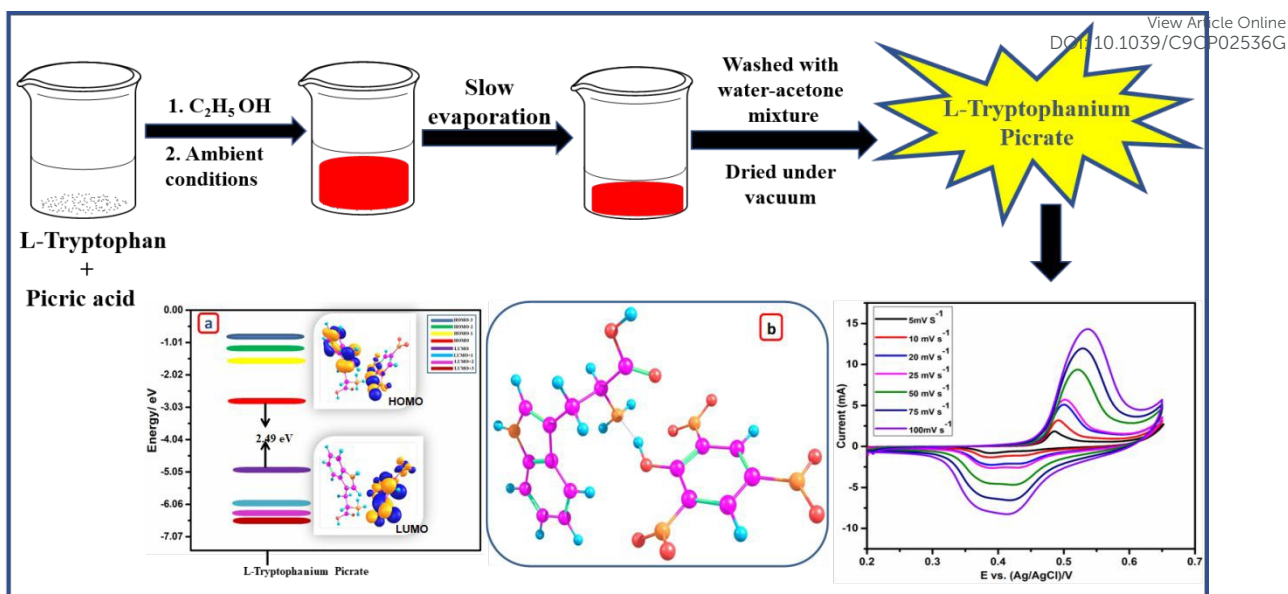
View Article Online
DOI: 10.1039/C9CP02536G

1. L. Dai, D. W. Chang, J. B. Baek and W. Lu, *Small*, 2012, **8**, 1130-1166.
2. A. S. Arico, P. Bruce, B. Scrosati, J.-M. Tarascon and W. Van Schalkwijk, *Mater. Sustain. Energy*, 2011, **4**, 148-159.
3. P.-C. Chen, G. Shen, Y. Shi, H. Chen and C. Zhou, *ACS Nano*, 2010, **4**, 4403-4411.
4. J. R. Miller and P. Simon, *Science Magazine*, 2008, **321**, 651-652.
5. W. Wei, L. Mi, S. Cui, B. Wang and W. Chen, *ACS Sustain. Chem. Eng.*, 2015, **3**, 2777-2785.
6. M. Winter and R. J. Brodd, *Chem. Rev.*, 2004, **104**, 4245-4270.
7. K. Chen and D. Xue, *ACS Appl. Mater. Interfaces*, 2016, **8**, 29522-29528.
8. A. R. Fiorucci and É. T. G. Cavalheiro, *J. Pharm. Biomed. Anal.*, 2002, **28**, 909-915.
9. T. B. Schon, B. T. McAllister, P.-F. Li and D. S. Seferos, *Chem. Soc. Rev.*, 2016, **45**, 6345-6404.
10. Z. Liu, G. Liang, Y. Zhan, H. Li, Z. Wang, L. Ma, Y. Wang, X. Niu and C. Zhi, *Nano Energy*, 2019, **58**, 732-742.
11. R. Hastak, P. Sivaraman, D. Potphode, K. Shashidhara and A. Samui, *Electrochim. Acta*, 2012, **59**, 296-303.
12. B. C. Patra, S. Khilari, L. Satyanarayana, D. Pradhan and A. Bhaumik, *Chem. Commun.*, 2016, **52**, 7592-7595.
13. Y. Huang, J. Tao, W. Meng, M. Zhu, Y. Huang, Y. Fu, Y. Gao and C. Zhi, *Nano Energy*, 2015, **11**, 518-525.
14. H. Jeong, H. J. Kim, Y. J. Lee, J. Y. Hwang, O.-K. Park, J.-H. Wee, C.-M. Yang, B.-C. Ku and J. K. Lee, *Mater. Lett.*, 2015, **145**, 273-278.
15. F. Wolfart, B. M. Hryniewicz, L. F. Marchesi, E. S. Orth, D. P. Dubal, P. Gomez-Romero and M. Vidotti, *Electrochim. Acta*, 2017, **243**, 260-269.
16. Z. Song and H. Zhou, *Energy Environ. Sci.*, 2013, **6**, 2280-2301.
17. Ö. A. Yokuş, F. Kardaş, O. Akyıldırım, T. Eren, N. Atar and M. L. Yola, *Sens. Actuators B Chem.*, 2016, **233**, 47-54.
18. S. Gowri, T. U. Devi, D. Sajan, S. Bheeter and N. Lawrence, *Spectrochim. Acta A Mol. Biomol. Spectrosc.*, 2011, **81**, 257-260.
19. A. Petrosyan, M. Fleck and V. Ghazaryan, *Spectrochim. Acta A Mol. Biomol. Spectrosc.*, 2013, **104**, 486-491.

20. V. Ghazaryan, M. Fleck and A. Petrosyan, *Spectrochim. Acta A Mol. Biomol. Spectrosc.*, 2015, **136**, 743-750. View Article Online
DOI: 10.1039/C5CP02536G
21. V. Ghazaryan, G. Giester, M. Fleck and A. Petrosyan, *J. Mol. Struct.*, 2015, **1101**, 219-227.
22. D. Joshi, D. Kumar, A. K. Maini and R. C. Sharma, *Spectrochim. Acta A Mol. Biomol. Spectrosc.*, 2013, **112**, 446-456.
23. P. Vishnoi, S. Sen, G. N. Patwari and R. Murugavel, *New J. Chem.*, 2015, **39**, 886-892.
24. A. Divyashree and G. Hegde, *RSC Adv.*, 2015, **5**, 88339-88352.
25. A. Shafiee, M. M. Salleh and M. Yahaya, *Sains Malays.*, 2011, **40**, 173-176.
26. M. Frisch, *J. Chem. Phys.*, 1999, **110**, 2822.
27. C. Lee, W. Yang and R. G. Parr, *Physical Review B*, 1988, **37**, 785.
28. T. Ishida, H. Nagata, M. Doi, M. Inoue, M. W. Extine and A. Wakahara, *Chem. Pharm. Bull.*, 1993, **41**, 433-438.
29. R. Zarrougui, R. Hachicha, R. Rjab and O. Ghodbane, *J. Mol. Liq.*, 2018, **249**, 795-804.
30. A. Jänes, J. Eskusson, T. Thomberg, T. Romann and E. Lust, *J. Energy Chem.*, 2016, **25**, 609-614.
31. R. Zarrougui, R. Hachicha, R. Rjab, S. Messaoudi and O. Ghodbane, *RSC Adv.*, 2018, **8**, 31213-31223.
32. B. T. McAllister, T. B. Schon, P. M. DiCarmine and D. S. Seferos, *Polym. Chem.*, 2017, **8**, 5194-5202.
33. S. Paranthaman, S. Sampathkumar and N. Murugasenapathi, *J. Chem. Sci.*, 2018, **130**, 164.
34. A. Szemik-Hojniak, K. Oberda, I. Deperasińska, Y. P. Nizhnik and L. Jerzykiewicz, *Polyhedron*, 2015, **88**, 190-198.
35. R. M. Silverstein, F. X. Webster, D. J. Kiemle and D. L Bryce, *Spectrometric Identification of Organic Compounds*, John Wiley & Sons, Hoboken, 2014.
36. T. Dhanabal, V. Tharanitharan, G. Amirthaganesan and M. Dhandapani, *Spectrochim. Acta A Mol. Biomol. Spectrosc.*, 2014, **128**, 694-700.
37. D. Arthi, E. Ilango, M. Mercina, D. Jayaraman and V. Joseph, *J. Mol. Struct.*, 2017, **1127**, 156-163.
38. A. González, E. Goikolea, J. A. Barrena and R. Mysyk, *Renew. Sustain. Energ Rev.*, 2016, **58**, 1189-1206.
39. X. Liu, Y. Gao and G. Yang, *Nanoscale*, 2016, **8**, 4227-4235.
40. M. Liao, Y. Liu, Z. Hu and Q. Yu, *J. Alloys Compd.*, 2013, **562**, 106-110.
41. F. Zhang, Y. Bao, S. Ma, L. Liu and X. Shi, *J. Mater. Chem. A Mater.*, 2017, **5**, 7474-7481.

42. D. Hulicova, J. Yamashita, Y. Soneda, H. Hatori and M. Kodama, *Chem. Mater.* **2005**, *17*, 1241-1247. DOI: 10.1039/C5CP02356G
43. M. Zhi, C. Xiang, J. Li, M. Li and N. Wu, *Nanoscale*, 2013, **5**, 72-88.
44. S. Bose, T. Kuila, A. K. Mishra, R. Rajasekar, N. H. Kim and J. H. Lee, *J. Mater. Chem.*, 2012, **22**, 767-784.
45. T. Kuila, P. Khanra, N. H. Kim, S. K. Choi, H. J. Yun and J. H. Lee, *Nanotechnology*, 2013, **24**, 365706.
46. P. Ramakrishnan and S. Shanmugam, *J Power Sources*, 2016, **316**, 60-71.
47. Y. Zhang, B. Lin, Y. Sun, X. Zhang, H. Yang and J. Wang, *RSC Adv.*, 2015, **5**, 58100-58106.
48. C. R. DeBlase, K. E. Silberstein, T.-T. Truong, H. D. Abruña and W. R. Dichtel, *J. Am. Chem. Soc.*, 2013, **135**, 16821-16824.
49. S. Chai, N. Hu, Y. Han, X. Zhang, Z. Yang, L. Wei, L. Wang and H. Wei, *RSC Adv.*, 2016, **6**, 49425-49428.
50. Y. Y. Kannangara, U. A. Rathnayake and J.-K. Song, *Chem. Eng J.*, 2019, **361**, 1235-1244.
51. S. Liu, L. Yao, Y. Lu, X. Hua, J. Liu, Z. Yang, H. Wei and Y. Mai, *Mater. Lett.*, 2019, **236**, 354-357.
52. A. Roy, S. Mondal, A. Halder, A. Banerjee, D. Ghoshal, A. Paul and S. Malik, *Eur. Polym. J.*, 2017, **93**, 448-457.
53. Z. Zhou, X. Zhang, L. Xing, J. Liu, A. Kong and Y. Shan, *Electrochim. Acta*, 2019, **298**, 210-218.
54. N. S. Punde, C. R. Rawool, A. S. Rajpurohit, S. P. Karna and A. K. Srivastava, *Chemistry Select.*, 2018, **3**, 11368-11380.
55. A. Zolfaghari, H. R. Naderi and H. R. Mortaheb, *J. Electroanal. Chem.*, 2013, **697**, 60-67.
56. Y. Ren, Q. Xu, J. Zhang, H. Yang, B. Wang, D. Yang, J. Hu and Z. Liu, *ACS Appl. Mater. Interfaces*, 2014, **6**, 9689-9697.
57. N. Li, Z. Xu, Y. Liu and Z. Hu, *J. Alloys Compd.*, 2019, **789**, 613-621.
58. N. Li, Z. Xu, Y. Liu and Z. Hu, *J. Power Sources*, 2019, **426**, 1-10.
59. Y. Y. Kannangara, U. A. Rathnayake and J.-K. Song, *Electrochim. Acta*, 2019, **297**, 145-154
60. D. Xue, D. Zhu, W. Xiong, T. Cao, Z. Wang, Y. Lv, L. Li, M. Liu, L. Gan, *ACS Sustain. Chem. Eng.*, 2019, **7**, 7024-7034.

61. L. Miao, X. Qian, D. Zhu, T. Chen, G. Ping, Y. Lv, W. Xiong, Y. Liu, L. Gan, M. Liu, *Chinese Chem. Lett.*, DOI: 10.1016/j.ccl.2019.03.010..
62. L. Hu, L. Ma, Q. Zhu, L. Yu, Q. Wu, C. Hu, N. Qiao and B. Xu, *New J. Chem.*, 2017, **41**, 13611-13618.
63. Y. Wang, L. Zhao, H. Peng, X. Dai, X. Liu, G. Ma and Z. Lei, *Ionics*, 2019, 1-9.
64. K. R. Reddy, B. Hemavathi, G. R. Balakrishna, A. Raghu, S. Naveen and M. Shankar, *Polymer Composites with Functionalized Nanoparticles*, Krzysztof Pielichowski and Tomasz M. Majka, Elsevier, Netherlands, First Edition, 2019, 357-379.
65. S. Huo, M. Liu, L. Wu, M. Liu, M. Xu, W. Ni and Y.-M. Yan, *J Power Sources.*, 2019, **414**, 383-392.
66. B.-H. Cheng, F.-X. Zeng, W.-J. Chen, H.-Y. Cheng, R. J. Zeng and H. Jiang, *iScience*, 2019, **12**, 204-215.



L-Tryptophanium picrate was synthesized and evaluated for its supercapacitor behavior and 263 F g⁻¹ of specific capacitance was achieved.